HHS Public Access

Author manuscript

Biomaterials. Author manuscript; available in PMC 2016 June 01.

Published in final edited form as:

Biomaterials. 2015 June ; 52: 426–440. doi:10.1016/j.biomaterials.2015.02.064.

Emulating Native Periosteum Cell Population and Subsequent Paracrine Factor Production To Promote Tissue Engineered Periosteum-Mediated Allograft Healing

Michael D. Hoffman and

University of Rochester, Department of Biomedical Engineering, University of Rochester Medical Center, Center for Musculoskeletal Research, 207 Robert B. Goergen Hall, Box 270168, Rochester, NY 14627-0168

Danielle S.W. Benoit

James P. Wilmot Distinguished Assistant Professor, University of Rochester, Departments of Biomedical Engineering, Chemical Engineering, University of Rochester Medical Center, Department of Orthopaedics, and Center for Musculoskeletal Research, 207 Robert B. Goergen Hall, Box 270168, Rochester, NY 14627-0168

Michael D. Hoffman: hoffman@bme.rochester.edu; Danielle S.W. Benoit: benoit@bme.rochester.edu

Abstract

Emulating autograft healing within the context of decellularized bone allografts has immediate clinical applications in the treatment of critical-sized bone defects. The periosteum, a thin, osteogenic tissue that surrounds bone, houses a heterogeneous population of stem cells and osteoprogenitors. There is evidence that periosteum-cell derived paracrine factors, specifically vascular endothelial growth factor (VEGF) and bone morphogenetic protein 2 (BMP2), orchestrate autograft healing through host cell recruitment and subsequent tissue elaboration. In previous work, we demonstrated that the use of poly(ethylene glycol) (PEG) hydrogels as a tissue engineered (T.E.) periosteum to localize mesenchymal stem cells (MSCs) to the surface of decellularized bone enhances allograft healing and integration. Herein, we utilize a mixed population of 50:50 MSCs and osteoprogenitor cells to better mimic native periosteum cell population and paracrine factor production to further promote allograft healing. This mixed cell population was localized to the surface of decellularized allografts within degradable hydrogels and shown to expedite allograft healing. Specifically, bone callus formation and biomechanical graft-host integration are increased as compared to unmodified allografts. These results demonstrate the dual importance of periosteum-mediated paracrine factors orchestrating host cell recruitment as well as new bone formation while developing clinically translatable strategies for allograft healing and integration.

Correspondence to: Danielle S.W. Benoit, benoit@bme.rochester.edu.

Disclosure: all authors state that they have no conflicts of interest

Keywords

cell transplantation; mesenchymal stem cells; hydrogels; bone allografts; periosteum; poly(ethylene glycol)

1. Introduction

The importance of the periosteum in coordinating autograft healing and repair is well established [1–8]. The cells of the periosteum, particularly periosteal stem cells and osteoprogenitors directly contribute to initial callus production, as well as through paracrine activation and recruitment of host cells [5, 8–10]. Using lineage-tracing techniques and murine femoral defect models, peak autograft callus formation occurs ~ 21 days post-implantation, during which time initial donor periosteum-mediated cartilaginous matrix production is replaced by host-derived mineralized tissue [10]. Furthermore, removal of the periosteum results in a 63% decrease in new bone formation during autograft healing and repair [10, 11]. Similarly, decellularized bone allografts, the clinical “gold standard” of treatment for critical sized bone defects, exhibit a comparable 61% decrease in bone formation as compared to autografts [12]. As previously noted, removal of the periosteum, as is the case in decellularized allografts, not only results in the removal of critical stem cell and osteoprogenitor cell populations, but also the growth factors produced by these cells [1–8]. Following injury, bone lining cells, circulating platelets, and peripheral cell populations release growth factors, including bone morphogenetic proteins (BMPs), fibroblast growth factor (FGF), insulin-like growth factor (IGF), platelet derived growth factor (PDGF), transforming growth factor-β (TFG-β), and vascular endothelial growth factor (VEGF) [1, 5, 8, 9, 13]. In particular, the cells of the periosteum have been shown to secrete large quantities of VEGF and BMP2 following injury [14–19]. In addition, MSCs, which are phenotypically comparable to periosteal stem cells, exhibit comparable paracrine factor expression [5, 20].

VEGF and BMP2 play critical roles in initiating and regulating bone healing, and successful remodeling requires precise activation and temporal expression of these factors [13, 21–25]. In the context of autografts, VEGF is critical in the early phases of healing and induces angiogenesis, vascular sprouting, and capillary permeability [8, 26]. BMP2 plays a role in later healing events, regulating matrix mineralization and new bone formation through both intramembranous and endochondral ossification [13, 23, 27, 28]. VEGF and BMP2 also act synergistically during early angiogenesis and matrix mineralization to promote cellular proliferation, callus formation, and generation of cell populations necessary for endochondral ossification [25, 26, 29–31]. In an effort to emulate autograft healing in the context of decellularized bone allografts, numerous strategies have investigated growth factor delivery strategies [10–12, 32–37]. In particular, dual delivery of VEGF and BMPs has been commonly employed to synergistically enhance bone production with variable success [10–12, 32–40]. However, exogenous administration of growth factors is complicated by diffusion and degradation, as well as the supraphysiological doses required for biological effects that may lead to off-target pathway activation [23, 41, 42]. As an

example, Cao *et al*. demonstrated enhanced repair within a rabbit segmental defect model via transplantation MSCs overexpressing ANG1 [43].

To overcome complications associated with the delivery of exogenous growth factors, some approaches have focused on transplantation or recruitment of cells to promoted allograft revitalization by producing cues for healing and repair [5, 8, 13, 21, 44]. [12, 36]. Long *et al*. augmented decellularized allografts with MSC cell sheets and demonstrated significant enhancements in callus bone formation and allograft healing and integration 6 weeks post-implantation [36]. The healing was attributed to transplanted MSCs, which are known to secrete myriad soluble factors that are critical for healing, including, but not limited to VEGF, BMP2, angiopoietin 1 (ANG1), and stromal-derived factor-1 (SDF1) [1, 13, 21, 45–48]. To better mimic native autograft cell populations and subsequent paracrine factor production, *ex vivo* MSC differentiation strategies have also been utilized prior to MSC transplantation [1, 13, 33]. For example, Ma *et al*. transplanted osteoblasts derived from MSCs to enhance bone formation within a rabbit mandible defect [33]. Similarly, transplantation of osteoblasts to critical sized calvarial defects were able to activate host MSCs, resulting in enhanced bone formation and healing [49]. Although these studies did not longitudinally track transplanted cell, the data suggests that *ex vivo* phenotypic modulation of transplanted cells enhances healing, possibly through modified paracrine factor production.

Previously, we demonstrated that PEG-based hydrogels can be used to localize MSCs to the surface of decellularized bone allografts [4, 12]. T.E. periosteum-modified allografts result in significant increases in graft vascularization, bone callus formation, and biomechanics, as compared to unmodified allograft controls 16 weeks post-implantation in a segmental femoral defect model [12]. Despite the observed increases in healing, endochondral ossification was significantly delayed compared to autograft controls [12]. In an effort to expedite the rate of endochondral ossification, enhance the rate of allograft healing and integration, and further emulate the dual functionality of the native tissue, the T.E. periosteum transplanted cell population was modified to mimic the native periosteum cell population and subsequently native autograft paracrine factor production [2, 3, 5–7]. Towards this end, a subset of MSCs were differentiated into osteoprogenitor cells, combined with unaltered MSCs in a 50:50 mixture, and transplanted *in vivo* to create a T.E. periosteum to more closely emulate native periosteum-mediated healing observed in autografts [12, 33].

2. Materials and Methods

All materials were purchased from Sigma-Aldrich unless otherwise specified.

2.1 Synthesis of Poly(ethylene glycol) (PEG) Macromolecular Monomers (Macromers)

Hydrolytically Degradable PEG Macromers—Hydrolytically degradable, PEG-based tri-block copolymers PEGPLADM (methacrylate-poly(lactide)-b-PEG-b-poly(lactide)-methacrylate) (Fig. 1A), were synthesized by functionalizing linear PEG (Alfa Aesar, MW 10 kDa) with *d,l*-lactide and performing microwave-assisted methacrylation, as previously described [12, 50–53]. ^{1}H-NMR analysis (Bruker Avance 400 MHz, $CDCl_3$) was used to determine the number of lactide units (m=3) and methacrylate functionality (>95%) per PEG

macromer. (-CH_2CH_2O- (PEG), 908H, 3.2–3.8 ppm, multiplet; -OCH(CH_3)COO-, 4H/PLA repeat, 5.2–5.3 ppm, multiplet; -OCH(CH_3)COO-, 12H/PLA repeat, 1.4–1.6 ppm, multiplet; CH_2=C(CH_3)-, 4H/macromer, 5.6 and 6.3 ppm, singlets; CH_2=C(CH_3)-, 6H/macromer, 1.9 ppm, singlet).

Synthesis of Acrylate-PEG-RGDS—The cell adhesive sequence Arg-Gly-Asp-Ser (Fig. 1; RGDS; 433 Da, EMD Chemicals, San Diego CA) was coupled to acrylate-PEG-N-Hydroxysuccinimide (Jenkem Technology, Beijing China, MW 3500 Da, p=79) through the amino terminus to allow for incorporation into hydrogels, as previously described [12, 51]. The product (Acrylate-PEG-RGDS, Fig. 1) was dialyzed against deionized water (molecular weight cutoff = 1000 Da, Spectrum Labs, Rancho Dominguez CA), lyophilized, analyzed via matrix-assisted laser desorption/ionization-time of flight mass spectrometry (MALDI-TOF, Bruker AutoFlex III SmartBeam); (solvent: 50% acetonitrile in H_2O + 0.1% TFA; matrix: α-cyano-4-hydroxy cinnamic acid (TCI Europe); calibrant: Peptide Calibration Standard (Bruker, #206195)) (*m/z Cl-*, 3854 Da), and stored at 4 °C.

2.2 Cell Culture

Bone marrow derived mouse MSCs expressing green fluorescent protein (GFP^+ mMSCs) isolated from GFP transgenic mice (C57BL/6-Tg(UBC-GFP)30Scha/J) were obtained from the mesenchymal stem cell distribution center at Texas A&M (passage 6) [54]. GFP^+ mMSCs were grown at 37 °C and 5% CO_2 in growth media consisting of Iscove's Modified Dulbecco's Medium (IMDM, Gibco) supplemented with 10% Fetal Bovine Serum (FBS), 10% horse serum (Atlanta Biologicals, Lawrenceville, GA, USA), 100 units/ml penicillin (Lonza), 100 μg/ml streptomycin (Lonza), and 0.25 μg/ml amphotericin B (Lonza). Where indicated, GFP^+ mMSCs were differentiated into osteoprogenitors via standard osteogenic induction media for a period of 10 days [33, 55] (e.g., low-glucose Dulbecco's Modified Eagle Medium (DMEM, Thermo) supplemented with 10% FBS, 100 units/ml penicillin, 100 μg/ml streptomycin, 0.25 μg/ml amphotericin B, 100 nM dexamethasone, 10 mM β-glycerophosphate, and 50 μM ascorbic acid-2-phosphate (2-phospho-L-ascorbic acid)). Osteogenic differentiation of MSCs was confirmed via gene expression analysis and histological staining [51]. GFP^+ mMSCs were used prior to passage 10.

2.3 Bone Graft Preparation and Transplantation

Mouse Strains—Female 6–8 week old C57BL/6 mice were purchased from Taconic (Hudson, NY). Allogeneic bone grafts for implantation into C57BL/6 mice were dissected from freshly euthanized, age-matched wild-type BALB/c mice obtained from various research groups within the University of Rochester Medical Center.

Murine Segmental Femoral Graft Model—*In vivo* healing of bone grafts was assessed using a previously established murine segmental femoral graft model [10–12, 56]. Briefly, 6–8 week old C57BL/6 mice were anesthetized via an intraperitoneal injection of ketamine and xylazine (60 mg/kg and 4 mg/kg, respectively). An 8 mm long incision was made, and blunt dissection was used to expose the mid-shaft of the femur. A Dremel with a diamond blade attachment was then used to remove a 5 mm mid-diaphyseal segment from the femur. A 5 mm cortical bone graft (autografts, allografts, or T.E. periosteum modified allografts)

was transplanted into the femur defect and stabilized using a 22-gauge intramedullary pin. For autograft transplantation, the graft was carefully dissected to maintain an intact periosteum, and immediately transplanted back into the same mouse. For devitalized bone allograft transplantation, the grafting procedure was performed between mice with genetically different backgrounds. Allografts were scraped to remove periosteal tissue, flushed repeatedly with phosphate buffered saline (PBS) to remove marrow, sterilized with 70% ethanol, rinsed in PBS to remove residual ethanol, and stored at −80 °C for at least 1 week prior to transplantation. All animal surgery procedures were performed under protocols approved by The University of Rochester Committee of Animal Resources (UCAR).

Cell Photoencapsulation in PEG Hydrogels Around Decellularized Allografts: The Tissue Engineered Periosteum—A 10 wt% solution of PEGPLADM was prepared in PBS with 2.0 mM Acrylate-PEG-RGDS (Fig. 1A). RGDS is included as previous studies have shown integrin interactions are important for maintenance of MSC viability [57–59]. The photoinitiator lithium phenyl-2,4,6-trimethylbenzoylphosphinate (LAP) was synthesized as previously described [60], and added to the PEG+RGDS solution at a final concentration of 0.05 wt%. Trypsinized MSCs (undifferentiated, osteogenic, or a 50:50 combination thereof) were added to the PEG macromer solution to achieve a final total concentration of 25 million cells/mL. As previously described [4], a custom mold was used to form tissue engineered (T.E.) periosteum modified allografts (Fig. 1). Briefly, 20 μL of PEG/cell solution was pipetted into cylindrical molds containing allografts and exposed to long-wavelength 365 nm light (5 mW/cm^2 intensity) for 10 min at room temperature to form uniform PEG/cell hydrogel coatings with >95% cell viability [57, 61]. It should be noted that the resultant 0.5 million cells localized to the graft surface is comparable to the periosteal cell density observed during autograft healing and repair.

Assessment of Encapsulated MSC-Mediated Paracrine Factor Release—T.E. periosteum modified allografts encapsulating MSCs, osteogenic MSCs, or a 50:50 combination thereof, as well as unmodified allografts and excised autograft controls were cultured in 24-well plates containing growth media for a period of 24 hours. Growth media was subsequently collected and vascular endothelial growth factor (VEGF), bone morphogenetic protein-2 (BMP2), angiopoietin 1 (ANG1), and angiopoietin 1 (ANG2) was quantified on a per-graft basis using enzyme-linked immunosorbent assays (ELISA) (VEGF and BMP2 Quantikine ELISA Kits; R&D Systems; Minneapolis, MN, ANG1 and ANG2 MyBioSource ELISA Kits; San Diego, CA).

2.4 Analysis of *In Vivo* Bone Graft Healing

Assessing Transplanted MSC Gene Expression via Laser Capture Microdissection—Following T.E. periosteum modified allograft transplantation, mice designated for laser capture microdissection (LCM) were fixed with 4% paraformaldehyde (PFA), prepared in diethylpyrocarbonate (DEPC) treated water to preserve RNA quality, via intravenous perfusion at either 1.5, 3, 6, or 9 weeks, as previously described [12, 62]. DEPC treated water was prepared at 0.001% v/v, stirring overnight, and autoclaving to inactivate DEPC prior to use. Following tissue fixation, T.E. periosteum modified allografts were

harvested and decalcified in 14% ethylenediaminetetraacetic acid (EDTA) overnight. Samples were then incubated for 24 hours each in 10%, 20%, and 30% solutions of sucrose in phosphate buffered saline (PBS), and embedded in optimal cutting temperature compound (Tissue-Tek OCT Compound; Sakura Finetek; Torrance, CA) [63]. Sections (5 μm) were cut using the CryoJane Tape Transfer System (Leicra Biosystems; Buffalo Grove, IL) on a Shandon Crytome FE (Thermo Scientific; Waltham, MA) and stored at −80 °C until LCM was performed [63]. A total of 15 sections (5 sections at 3 different levels) were obtained for each specimen. Immediately prior to LCM, sections were stained with hematoxylin (blue, basophilic cytoplasm/nuclei). LCM was performed using a Zeiss Palmbeam Laser Capture Microdissection Microscope (Zeiss; Oberkochen, Germany) and fluorescence microscopy was utilized to verify that only transplanted GFP^+ mMSC were captured.

Reverse-transcription polymerase chain reaction (RT-PCR) was used to assess gene expression of transplanted GFP^+ mMSCs collected via LCM. Sample RNA was isolated using the QIAGEN RNeasy Kit (Qiagen; Valencia, CA) and RNA concentrations were normalized across groups to account for variations in the number of collected cells. RT was performed using the iScript cDNA Synthesis Kit (Bio-Rad; Hercules, CA) incubated at 25 °C for 5 min, 42 °C for 30 min, and terminated at 85 °C for 5 min. PCR was performed using a CFX96 Real-Time PCR System (Bio-Rad, SsoFastEvaGreen Master Mix). Primers for β-actin, runt-related transcription factor 2 (Runx2, also known as core-binding factor subunit alpha-1, Cbfa1), alkaline phosphatase (ALP), sex determining region Y-box 9 (Sox9), alpha-1 type-1 collagen (Col1a1), vascular endothelial growth factor (VEGF), and bone morphogenetic protein-2 (BMP2) were used. Primer sequences utilized are listed in Table S1 [64–67]. The PCR parameters used were as follows: hold at 95 °C for 5 min, followed by 40 cycles of: 95 °C for 15 sec denaturation, 60 °C (55 °C for BMP2) for 60 sec annealing, and 72 °C for 20 sec extension. Threshold cycle (C_T) analysis was used to quantify PCR products normalized to the housekeeping gene β-actin. Relative gene quantification was performed using the Pfaffl Method, taking into account the variation between primer efficiencies [68].

Histological Staining and Histomorphometric Analysis—Femur grafts were harvested, and alcian blue (blue, glycosaminoglycans/proteoglycans) and orange G (pink, bone/soft tissue) stained sections were prepared as previously described [12]. At least three nonconsecutive sections were prepared from each specimen and imaged at 40x magnification using an Olympus VS110 Virtual Microscopy System for whole-slide scanning. Subsequently, histomorphometric analysis of bridging callus formation was carried out using Visiopharm software (Visiopharm, Denmark). Briefly, a 7 mm region of interest (ROI) was selected spanning the entire 5 mm graft with 1 mm of host overlap proximally and distally. The graft itself was removed from the selected ROI and only bridging callus on the surface of the graft and host bone was quantified. Mesenchyme, cartilage, and woven bone area were reported based on color threshold intensities and means of 3 nonconsecutive sections were averaged and used to represent area values for each graft.

Immunohistochemical Labeling—To visualize transplanted GFP^+ mMSCs, paraffin embedded sections (5 μm) of grafted femurs were immunostained using a polyclonal anti-

GFP antibody, as previously described [12]. Briefly, slides were deparaffinized, quenched of endogenous peroxidase activity (DAKO Dual Endogenous Enzyme Blocking Reagent; DAKO S2003), and blocked with 5% normal rabbit serum (NRS) (Vectastatin ABC Kit, Vector Laboratories, Burlingame, CA). Slides were incubated with goat polyclonal anti-GFP antibody (1:1500 dilution; #ab6673, Abcam Inc., Cambridge, MA) in 3% NRS in phosphate buffered saline with Tween-20 (PBST) overnight at 4 °C. Slides were then washed and then incubated in biotinylated rabbit anti-goat antibody (1:200 dilution; BA-5000, Vector Laboratories) in PBST, washed, and incubated with Vectastain ABC reagent. Finally, slides were developed using a Vector Impact DAB Kit and counter-stained for 1 min using hematoxylin (Invitrogen).

To qualitatively analyze vascularization during healing, paraffin embedded sections (5 μm) of grafted femurs were immunostained for CD31 (platelet endothelial cell adhesion molecule; PECAM). Briefly, slides were deparaffinized and proteolytically digested using proteinase K (# S3004, DAKO, Carpinteria, CA). Slides were incubated with rat monoclonal anti-CD31 antibody (1:100 dilution; #CM303, Biocare Medical, Concord, CA) in 5% normal goat serum (NGS) in UltraClean dilutent (#TA125UC, Thermo Fisher Scientific, Waltham, MA) for 90 min at room temperature. Finally, slides were developed using GBI Polymer HRP for Rat antibody (#D46–18, Golden Bridge International, Bothell, WA) and a KPL TrueBlue Chromagen Kit (#71-00-65, KPL, Gaithersburg, MD) and counter-stained for 5 min using nuclear fast red.

Quantification of Bone Callus Volume using Micro-Computed Tomography (μCT)—Analysis of bone callus volume was preformed using a μCT imaging system (Explore; GE HealthCare), as previously described [10, 12, 69]. Briefly, two-dimensional (2D) images were reconstructed and an appropriate threshold was selected for bone voxels. Both the threshold and volume of interest (VOI) were kept constant throughout the analysis of all femur specimens. To measure new bone callus volume, contour lines were drawn in the 2D images to exclude both the transplanted bone graft and the host cortical bone. New bone callus volume in a VOI spanning the entire length of the transplanted bone graft and 1 mm of the proximal and distal host cortical bone was used to evaluate graft healing.

Quantification of Vascularization using Micro-Computed Tomography—Host-mediated graft vascularization was examined using μCT analysis after vascular perfusion with a radiopaque lead chromate silicon rubber contrast agent (Microfil MV-122, Flow Tech; Carver, MA), as previously described [12, 62]. Following perfusion, femur specimens were isolated and scanned using μCT to image both vascularization and mineralized bone. Samples were subsequently decalcified (10% EDTA, 14 days) and scanned again to image only the remaining vasculature. 2D slices were registered before and after decalcification and contour lines were drawn to isolate a VOI that only included the vasculature within or immediately adjacent to the bone graft or the graft-host junctions.

Assessment of Graft Torsional Biomechanics—The proximal and distal ends of harvested femur specimens were cemented into 6.35 mm square aluminum tubes using bone cement prepared to the manufactures specifications (DePuy Endurance; Warsaw, IN). A custom jig was used to ensure axial alignment and the maintenance of a 7 mm gauge length

for all samples. Samples were mounted on an EnduraTec TestBench system (200 N-mm torque cell; Bose Corp., Minnetonka, MN) and tested in torsion until failure to determine ultimate torques [11, 12, 70].

Union Ratio Calculation—The union between host callus and transplanted bone graft was calculated from μCT images as previously described [12, 71]. For each graft, the reconstructed image was split into proximal and distal halves and the associated graft-host connectivity was calculated. The total graft-host connected surface area for each half was divided by the total graft surface area associated with the half in question. The union ratio for the total graft was defined as the lesser of the proximal and distal connectivity ratios.

2.5 Statistical Analysis

Data is presented as mean ± standard error of the mean, unless otherwise noted, with at least five replicates averaged for each data point. Statistics were assessed with GraphPad Prism Software using two-way ANOVAs with Bonferroni post-hoc analysis or paired Student's t-tests. A *p*-value of less than 0.05 was considered significant.

3. Results

3.1 Mimicking Autograft Paracrine Production within T.E. Periosteum Modified Allografts

Previously, we demonstrated that T.E. periosteum modified allografts transplanting MSCs alone exhibited increased healing compared to unmodified allografts. However, endochondral ossification was significantly delayed compared to autograft controls [12]. In addition, it has been demonstrated that paracrine factors from the periosteum are important for autograft repair [8, 22, 44, 72]. To expedite the rate of allograft healing and integration within T.E. periosteum modified allografts, and further emulate the dual functionality of native periosteal cells, the transplanted MSC population was modified to provide similar cellular and paracrine factor stimulation of healing as autograft controls. Therefore, a subset of MSCs were exposed to standard osteogenic culture conditions for a period of 10 days to generate osteoprogenitors [33]. Osteoprogenitors exhibited significantly increased expression of osteogenic markers Runx2 (2.9-fold; Fig. 2A) and ALP (4.9-fold; Fig. 2B), as well as mineralized matrix production (Fig. 2C; von Kossa, hydroxyapatite), as compared to MSC controls. Utilizing our previously described methods [12], T.E. periosteum modified allografts were subsequently fabricated localizing a 50:50 mixture of MSCs and osteoprogenitors (mixed) to the graft surface.

The production of vascular endothelial growth factor (VEGF) and bone morphogenetic protein-2 (BMP2) of autografts, allografts, and T.E. periosteum modified allografts were quantified *ex vivo* [1, 22, 24, 32, 73]. T.E. periosteum modified allografts including MSCs alone exhibit 2.2-fold (470.8 pg/mL/day) greater VEGF production, and a 4.9-fold (28.6 pg/mL/day) lower BMP2 production (Fig. 2D) compared to autograft controls. Furthermore, if osteoprogenitors are utilized in lieu of MSCs, there is a significant 2.6-fold (80.6 pg/mL/day) reduction in VEGF production, and 1.5-fold (206.3 pg/mL/day) greater BMP2 production (Fig. 2D). In contrast, allografts modified with a 50:50 mixture of MSCs and osteoprogenitors exhibit a 1.8-fold (386.7 pg/mL/day) greater VEGF production.

Furthermore, encapsulation of a mixed cell population within T.E.-periosteum modified allografts results in statistically comparable levels (1.1-fold greater; 156.3 pg/mL/day) of BMP2 production, as compared to autograft controls (Fig. 2D). Interestingly, VEGF produced by mixed cell populations (386.7 pg/mL/day) is 1.4-fold greater than the sum of the expected VEGF produced by MSCs (235.4 pg/mL/day) and osteoprogenitors (40.3 pg/mL/day). Similarly, BMP2 production by a mixed cell population is 1.3-fold greater than the sum of the expected BMP produced by mixtures of MSC and osteoprogenitor cell populations (14.3 and 103.2 pg/mL/day, respectively).

3.2 *In Vivo* Healing Efficacy of T.E. Periosteum

3.2.1 T.E. Periosteum-Mediated Vascularization—The *in vivo* healing efficacy of T.E. periosteum modified allografts was investigated within the context of a murine femur segmental defect model [4, 10–12]. Vascularization was examined as it is critical in the initiation of graft healing, and has been shown to be influenced by periosteal VEGF and BMP2 signaling, as well as other paracrine factors [24, 47, 74, 75]. To investigate the efficacy of transplanted MSCs on initiating this healing cascade, host-mediated vascular infiltration was assessed 6 and 9 weeks following implantation using contrast enhanced vascular perfusion and subsequent μCT-based reconstruction techniques (Fig. 3A) [12, 62]. Quantitative analysis of graft vascular volume demonstrated that compared to untreated allograft controls, T.E. periosteum-modified allografts transplanting only MSCs exhibited a 2.0- (0.9 mm^3) and 1.4-fold (0.9 mm^3) increase in vascular volume at 6 and 9 weeks post-implantation (Fig. 3B). In contrast, T.E. periosteum-modified allografts transplanting only osteoprogenitors exhibited a 2.5- (0.4 mm^3) and 1.9-fold (0.5 mm^3) reduction in vascular volume at 6 and 9 weeks post-implantation, as compared to transplantation of MSCs alone (Fig. 3B). Furthermore, T.E. periosteum-modified allografts transplanting a combination of MSCs and osteoprogenitors exhibited a 2.7- (0.3 mm^3) and 2.3-fold (0.4 mm^3) reduction in vascular volume at 6 and 9 weeks post-implantation, as compared to transplantation of MSCs alone (Fig. 3B). Further quantification revealed that at 6 weeks post-implantation, allografts modified with MSCs, osteoprogenitors, or a combination of MSCs and osteoprogenitors exhibited comparable vascular diameter distributions (Fig. 3Ci). However at 9 weeks post-implantation, allografts modified with either osteoprogenitors, or a combination of MSCs and osteoprogenitors exhibited a significant decrease in large vessel formation and a significant increase in small vessel formation (Fig. 3Cii). In addition, compared to allografts modified with MSCs, allografts modified with either osteoprogenitors, or a combination of MSCs and osteoprogenitors exhibited a qualitative decrease in vessel circumference and diameter within the bridging callus, as assessed via CD31+ staining (Fig. 3D), at both 6 and 9 weeks post-implantation. To further assess the underlying reason for the apparent shift from large vessel arteriogenesis to small vessel angiogenesis, per graft paracrine production of angiopoeietin 1 (ANG1), an inhibitor of large vessel arteriogenesis, as well as angiopoeietin 2 (ANG2), an inhibitor of small vessel arteriogenesis was quantified (Fig. 4A) [47, 48, 75–77]. While graft-mediated ANG2 production remained undetectable ANG1 was shown to be increased 3.6- and 2.1-fold in allografts modified with osteoprogenitors, or a mixed cell population, respectively, as compared to allografts modified with MSCs alone (Fig. 4B).

3.2.2 T.E. Periosteum-Mediated Bone Callus Formation—To further investigate how changes in T.E. periosteum-mediated paracrine production alters allograft healing, bone callus formation was quantified using μCT analysis 6 and 9 weeks post-implantation (Fig. 5). As previously demonstrated [12], autografts exhibit uniform callus formation with extensive graft resorption and the formation of a complete bridging bone collar (Fig. 5A). Autografts also exhibit a callus bone volume of 3.5 mm^3 6 weeks post-implantation and this volume decreases to 2.6 mm^3 by 9 weeks as a result of graft resorption and remodeling (Fig. 5B). In contrast to autografts, unmodified allografts exhibit a significant 2.6- (1.4 mm^3) and 1.3-fold (2.0 mm^3) decrease in callus bone formation at 6 and 9 weeks, respectively (Fig. 5B). In addition, allograft callus bone formation is localized only to the proximal and distal ends of the graft with a failure to form a completely bridged callus (Fig. 5A). T.E. periosteum modified allografts transplanting a mixture of MSCs and osteoprogenitors exhibit a significant 3.7- (5.0 mm^3) and 2.8-fold (5.7 mm^3) increase in bone callus formation 6 and 9 weeks post-implantation, as compared to unmodified allograft controls (Fig. 5B). Furthermore, bone callus formation of T.E. periosteum modified allografts transplanting a mixed cell population were 3.0- (1.66 mm^3) and 1.5-fold (3.8 mm^3) greater than transplantation of MSCs alone, and 1.2- (4.2 mm^3) and 1.4-fold (4.1 mm^3) greater than transplantation of osteoprogenitors alone, at 6 and 9 weeks respectively (Fig. 5B).

3.2.3 T.E. Periosteum-Mediated Bridging Callus and Endochondral Bone Formation—Histological sections were examined both 6 and 9 weeks after implantation to further elucidate how T.E. periosteum mediates callus bone formation (Fig. 6). As has been previously observed [12], autograft healing was marked by significant graft resorption, (Fig. 6A) and the simultaneous formation of a uniform bridging callus bone collar (Fig. 6B). In contrast to autografts, unmodified allografts fail to remodel (Fig. 6C–D). In addition, allografts do not generate a bridging callus bone collar; instead only minimal amounts of callus bone are formed at the proximal and distal graft-host interfaces (Fig. 6C) with complete resorption of callus occurring by 9 weeks (Fig. 6D). Unlike allografts, T.E. periosteum modified allografts transplanting MSCs (Fig. 6E–F), osteoprogenitors (Fig. 6G–H), or a mixture of MSCs and osteoprogenitors (Fig. 6I–J) exhibited a significant increase in bridging callus formation. In particular, T.E. periosteum modified allografts transplanting MSCs (Fig. 6E–F; black arrows) or osteoprogenitors (Fig. 6G–H; black arrows) exhibited significant increases in bridging cartilaginous matrix production, as indicated by alcian blue staining. In contrast, T.E. periosteum modified allografts transplanting a mixed cell population exhibited qualitatively comparable bridging callus formation but a significant reduction in bridging cartilaginous matrix production was observed (Fig. 6I–J; black arrows).

To quantify the marked increase in T.E. periosteum-mediated bridging callus formation, histomorphometric analysis was performed on alcian blue/orange G stained tissue sections (Fig. 6). Using colorimetric thresholding techniques, total callus area, as well as total mesenchyme, total cartilage, and total woven bone area were quantified (Fig. 7). Compared to unmodified allografts, T.E. periosteum modified allografts transplanting mixtures of MSCs and osteoprogenitors, MSCs, or osteoprogenitors exhibited statistically comparable 2.9- (10.9 mm^2) and 4.0-fold (10.7 mm^2), 2.6- (9.5 mm^2) and 3.5-fold (9.5 mm^2), and 2.8-

(10.1 mm^2) and 3.9-fold (10.5 mm^2) increases in total callus area, after 6 and 9 weeks of healing (Fig. 7A). Compared to unmodified allografts, T.E. periosteum modified allografts transplanting mixed cell population exhibited a 4.0- (Fig. 7B; 3.9 mm^2), 6.0-fold (Fig. 7C; 0.24 mm^2), and 3.4-fold (Fig. 7D; 6.5 mm^2) increase in total mesenchyme, cartilage, and woven bone area 9 weeks post-implantation. Furthermore, T.E. periosteum modified allografts transplanting a mixed cell population exhibited an 1.2- (Fig. 7B; 4.8 mm^2) and 6.3-fold (Fig. 7C; 1.5 mm^2) decrease in total mesenchyme and cartilage area compared to transplantation of MSCs only, and an 1.3- (Fig. 7B; 5.1 mm^2) and 5.9-fold (Fig. 7C; 1.4 mm^2) decrease in total mesenchyme and cartilage area compared to transplantation of osteoprogenitors only at 9 weeks post-implantation. In contrast, T.E. periosteum modified allografts transplanting mixtures of MSCs and osteoprogenitors exhibited a 2.1- (3.1 mm^2) and 1.6-fold (4.0 mm^2) increase in total woven bone area as compared to transplantation of MSCs or osteoprogenitors at 9 weeks post-implantation (Fig. 7D).

3.2.4 T.E. Periosteum-Mediated Allograft Biomechanical Stability—Torsion testing was performed 6 and 9 weeks post-implantation to assess the extent of graft host integration for the various T.E. periosteum. As observed previously [11, 12], autografts (31.2 and 31.9 N-mm) exhibited maximal torque values that were comparable to intact femurs (26.5 and 24.4 N-mm) controls, at both 6 and 9 weeks, respectively (Fig. 8). In contrast to autografts, unmodified allografts exhibited a statistically significant 7.8-fold (3.4 N-mm) and 7.2-fold (3.4 N-mm) decrease in maximal torque at 6 and 9 weeks (Fig. 8). Unlike allografts, T.E. periosteum modified allografts transplanting both MSCs and osteoprogenitors exhibit a significant 2.7-fold (9.0 N-mm) increase in maximal torque 9 weeks post-implantation, as compared to unmodified allografts (Fig. 8). Furthermore, maximal torque values for T.E. periosteum modified allografts transplanting a mixed cell population were 2.2-fold (4.1 N-mm) greater than transplantation of MSCs alone, and 1.9- (4.7 N-mm) greater than transplantation of osteoprogenitors alone, at 9 weeks, respectively (Fig. 8). Increased mechanical stability was further supported by increasing trends in graft-host connectivity, as determined by μCT-based union ratio calculations (Table. 1). While statistical significance was not achieved, T.E. periosteum modified allografts transplanting both MSCs and osteoprogenitors exhibited a 1.4- (13.9%), 1.2- (15.9%), and 1.3-fold (15.4%) increase in graft-host connectivity 9 weeks post-implantation, as compared to unmodified allografts and T.E. periosteum modified allografts transplanting only MSCs or osteoprogenitors.

3.2.5 In Vivo Gene Expression of T.E. Periosteum Transplanted Cells—To elucidate the cellular contributions of transplanted MSCs, gene expression was analyzed at 0, 1.5, 3, 6, and 9 weeks post-implantation. Immunohistochemical labeling of green fluorescent protein (GFP) showed that transplanted GFP^+ mMSCs exhibit minimal engraftment into newly formed bone callus (Fig. 9A). However, laser capture microdissection (Fig. 9B) and subsequent gene expression for transplanted cells revealed that mixed cell populations exhibited trends towards increases in markers of endochondral ossification (Fig. 9C). Although not statistically significant, compared to MSCs, the mixed population of transplanted MSCs exhibited a 1.6-fold increase in Sox9 expression 1.5 weeks post-implantation (Fig. 9Ci). Furthermore, by 9 weeks post-implantation the mixed

population of MSCs exhibited a significant 3.7-fold reduction in Sox9 expression as compared to MSCs (Fig. 9Ci). In addition, as Sox9 expression decreased within the mixed population of MSCs, Runx2 expression steadily increased, reaching 1.7-fold that of MSCs by week 9 (Fig. 9Cii). In contrast to MSCs, transplantation of a mixed population of MSCs resulted in a 4.9-fold increase in Col1a1 expression by week 3, before decreasing to a level that was comparable to MSC controls (Fig. 9Ciii).

Transplanted MSCs retained both VEGF (Fig. 9Civ) and BMP2 (Fig. 9Cv) expression. Compared to MSCs, transplantation of a mixed population of MSCs resulted in a 2.7-fold decrease and 3.9-fold increase in VEGF and BMP2 expression respectively, immediately following transplantation (Fig. 9Civ and 9Cv). This trend remained consistent through 9 weeks where transplantation of a mixed MSC population exhibited a 2.1-fold decrease and 1.8-fold increase in VEGF and BMP2 expression respectively, as compared to MSCs alone (Fig. 9Civ and 9Cv).

4. Discussion

4.1 Summary

The periosteum is critical in orchestrating autograft repair through direct tissue elaboration during initial callus production and paracrine-mediated host cell activation and recruitment [8, 13, 22, 23, 44, 72]. The focus of this study was to build upon our previous work developing a PEG-based T.E. periosteum [4, 12], and further modulate allograft healing by altering the transplanted MSC population to mimic both the cell population and paracrine factor elaboration of the native periosteum. Our results demonstrate that by biasing half of the transplanted MSC population into osteoprogenitors, T.E. periosteum-modified allografts exhibit comparable BMP2 production as autografts *ex vivo* and enhanced healing *in vivo*. In particular, when transplanted into a murine femoral segmental defect model, T.E. periosteum-modified allografts transplanting a combination of MSC and osteoprogenitors exhibit increased callus bone formation, graft-host integration, and biomechanics, compared to all other groups.

4.2 Stem cells and osteoprogenitors are critical modulators of bone healing

Unlike previous studies focused on transplanting single cell populations, mainly MSCs [12, 36, 49], the work herein focused on transplanting a mixture of periosteum-emulating MSCs and osteoprogenitors [2, 3, 5–7]. As previously discussed, transplantation of either MSCs or osteoblasts has been shown to promote bone formation, but to date, co-transplantation of these cell populations has not been a typical approach [12, 36, 49]. In the work presented herein, following *in vivo* transplantation, T.E. periosteum including MSCs and osteoprogenitors were shown to increase the rate of allograft healing. As demonstrated by histomorphometric analysis, T.E. periosteum transplantation of mixed MSC populations results in a 1.8-fold (6.5 mm^2) increase in total woven bone callus area over an otherwise additive enhancement anticipated from 50:50 mixed MSC (1.6 mm^2) and osteoprogenitor (2.0 mm^2) cells. Only in T.E. periosteum-modified allografts encapsulating mixed cell populations was there a significant transition of cartilaginous matrix to ossified tissue (Fig. 7C). Consistent with histological findings, gene expression of the mixed population showed

expedited progression through endochondral ossification (Fig. 9C). The process of endochondral ossification and the transition from cartilaginous matrix to mineralized woven bone is required for the healing of critical sized bone defects, a process largely mediated by periosteal cells [10]. Furthermore, we previously demonstrated that transplanted MSCs contributed directly to the initial callus production [12], suggesting that the introduction of an osteogenic cell population promotes matrix mineralization. Similarly, transplantation of osteogenic differentiated rabbit MSCs resulted in increased expression of markers of endochondral ossification, and a subsequent 2.1-fold increase in bone deposition, as determined by histological analysis 4 weeks after implantation into a rabbit mandibular defect [33]. These results support the hypothesis that the heterogenous periosteum cell population, consisting of both stem cells and osteoprogenitors, is critical for replicating autograft healing in the context of decellularized allografts.

4.3 Transplanted cell paracrine factors corrdinate bone healing

In addition to direct cell contributions to endochondral ossification, periosteal cell paracrine factors, including VEGF and BMP2, coordinate autograft healing and repair [13, 21–25]. While VEGF is an important regulator of angiogenesis, a critical step in bone remodeling, it also promotes ossification and new bone formation, functions that are synergistically enhanced by BMP2 [26, 39, 78–80]. Consistent with previous observations, transplantation of mixed MSC populations resulted in synergistic enhancements of both VEGF and BMP2 production, as compared to delivery of either MSCs or osteoprogenitors alone (Fig. 2D) [20, 25, 81]. Transplantation of only MSCs or osteoprogenitors resulted in production of 470.8 and 80.6 pg/mL/day of VEGF, respectively. Accounting for the contributions of half of each population, it would be expected that T.E. periosteum encapsulating a 50:50 mixed cell population would exhibit an average of 275.7 pg/mL/day of VEGF production, however, 386.7 pg/mL/day was observed, a 1.4-fold increase over averaged values. This is an insignificant reduction in VEGF production as compared to T.E. periosteum-modified allografts including MSCs alone. Similarly, transplantation of MSCs or osteoprogenitors alone resulted in production of 28.6 and 206.3 pg/mL/day of BMP2, respectively. Again, accounting for the contribution of half of each population, it would be expected that T.E. periosteum encapsulating a 50:50 mixed cell population would exhibit 117.5 pg/mL/day of BMP2 production, however, 156.3 pg/mL/day was observed, a 1.3-fold increase over expected levels. As previously highlighted, transplantation of a mixed cell population results in increased callus bone formation (Figures 5 & 7), graft-host integration (Figure 6 & Table 1), and biomechanics (Figure 8), compared to all other groups.

Similar to our observations, silk hydrogel-mediated release of VEGF alone resulted in ~60% less new bone area when compared to release of a combination of both VEGF and BMP2 in a rabbit maxillary sinus floor defect model [80]. VEGF and BMP2 co-delivery versus BMP2 alone results in a 1.8-fold increase in endochondral ossification within murine calvarial defect models [79]. In particular, BMP2 is critical for initial steps in fracture healing [82]; Yu *et al*. demonstrated that recombinant BMP2 treatment of non-stabilized tibial fractures expedited cartilage resorption and bone deposition during endochondral bone formation [35]. Similarly, allografts coated with self-complementary adeno-associated virus serotype 2.5 vector for BMP2 (scAAV2.5-BMP2) demonstrated a statistically significant 2.3-fold

increase in callus bone formation, and a 10.9-fold increase in torsional rigidity 6 weeks post-implantation, compared to allograft controls [83]. As shown *in vitro* (Fig. 2D) and *in vivo* (Fig. 9C) here, BMP2 is significantly lacking in T.E. periosteum-modified allografts encapsulating MSCs alone. Compared to T.E. periosteum-modified allografts transplanting a mixed cell population, transplantation of MSCs alone results in a 1.5-fold decrease in bone callus formation (3.8 mm^3 vs. 5.7 mm^3; Fig. 5B). Together, this demonstrates that the mixed cell population within T.E. periosteum may exhibit synergistic VEGF and BMP2 production, possibly due to paracrine/autocrine signaling, resulting in expedited mineralization and callus bone formation, leading to a subsequent increase in biomechanical stability and overall graft healing.

While the roles of VEGF and BMP2 are clear, there are other factors important for bone healing [26, 39, 78–80, 84]. For example, angiopoietins 1 and 2 (ANG1, ANG2), along with VEGF, regulate angiogenesis and vessel maturation, contributing to bone healing [47, 48, 75–77]. ANG2, in particular, destabilizes pericyte/endothelial cell interactions and promoting vascular remodeling and growth during large vessel arteriogenesis [76]. In contrast, ANG1, an ANG2 agonist, stabilizes pericyte/endothelial cell interactions and promotes vascular maturation in the late stages of angiogenesis [47]. Inhibition of ANG2 within a murine femoral segmental defect model via anti-angiopoietin-2 peptibody (L1-10) treatment was shown to enhance healing by increasing the number of small, interpenetrating vessels within the bridging callus [75]. Furthermore, osteoblast-specific ANG1 over-expression has been shown to increase bone mass [85]. These results support our observed increase in small vessel formation within T.E. periosteum-modified allografts including mixed cell populations, or osteoprogenitors alone (Fig. 3). Furthermore, observed increases in ANG1 by T.E. periosteum-modified allografts including mixed cell populations or osteoprogenitors (Fig. 4) is consistent with literature findings that an osteogenic cell population increases local ANG1 production, thereby inhibiting macroscopic vessel formation [75, 85]. These findings also suggest that an increase in small interpenetrating vessels, as verified by CD31 labeling, may be underrepresented by the lead contrast perfusion imaging techniques utilized herein, thereby contributing to observed decreases in overall vascular volume.

4.4 Replicating native periosteal cells results in promising allograft healing

Here, evidence is provided that by altering the phenotype of cells encapsulated within T.E. periosteum modified allografts to better replicate native periosteal cell populations and subsequent paracrine factor production, allograft healing and integration can be enhanced [4, 12]. As previously noted, T.E. periosteum coated allografts encapsulating a mixed cell population resulted in a statistically significant 1.5-fold increase in callus bone formation 9 week post-implantation (Fig. 5B) [12]. Furthermore, temporal progression through endochondral mediated matrix ossification was expedited, more closely following trends observed in autograft healing (Fig. 6 & 7). Compared to T.E. periosteum mediated transplantation of MSCs alone, transplantation of a mixed MSC population results in an increased rate of cartilaginous matrix resorption, ossification, and as a result, graft-host biomechanical integration, 9 weeks post-implantation (Fig. 8 & Table. 1). Specifically, the increase in torsional biomechanics achieved herein at 9 weeks utilizing a mixed MSC

population is 1.6-fold greater than our previously-reported biomechanical increases obtained 16 weeks post-implantation using MSCs only [12]. Taken together, this work demonstrates that by mimicking native periosteum cell population and subsequent paracrine expression profiles in T.E. periosteum-modified allografts, an enhanced rate of healing is achieved that is in line with autograft healing. While this modification does not fully restore allograft healing to the levels observed in autografts, it is a significant step towards emulating the critical structure-function relationship of the periosteum. In addition, this bottom-up design approach utilizing PEG hydrogels affords further modification to allow for controlled growth factor release, potentially further optimizing this therapeutic strategy [86–89].

5. Conclusion

By mimicking autograft cell populations and subsequent paracrine signaling within T.E. periosteum-modified allografts, and thereby further replicating the dual functionality of native periosteal stem cells, allograft healing and integration was enhanced, as compared to all other transplanted cell populations. Specifically, T.E. periosteum BMP2 production was matched to autograft controls. When T.E. periosteum-modified allografts encapsulating a mixed cell population to match autograft BMP2 production were transplanted into a murine femoral segmental defect model, bone callus formation, bridging endochondral bone formation, and biomechanical stability were significantly increased as compared to unmodified allograft controls. These results demonstrate that periosteum-mediated paracrine signaling is critical for graft healing and integration. Furthermore, the work presented herein has established a strong foundation for the development of clinically translatable, therapeutic, and increasingly efficacious strategies for the treatment of critical sized bone defects.

Supplementary Material

Refer to Web version on PubMed Central for supplementary material.

Acknowledgments

Funding for this research was received from the NIH (R01-AR064200), the Orthopaedic Research and Education Foundation/Musculoskeletal Transplant Foundation (OREF/MTF). MDH was supported in part by the NIH (T32-AR053459). Equipment, including the IVIS Live Animal Imaging System, Visiopharm software, and whole-slide scanner were purchased through NIH funds (S10-RR026542-01, P30-AR061307, and S10-RR027340-01). The GFP^+ mMSCs were provided by the Texas A&M Health Science Center College of Medicine Institute for Regenerative Medicine at Scott & White through a grant from the NIH (P40-RR017447). The authors also wish to thank Dr. Linda Callahan, Mike Thullen, Sarah Mack, Kathy Maltby, and Mary Georger for their assistance.

References

1. Malizos KN, Papatheodorou LK. The healing potential of the periosteum molecular aspects. Injury. 2005; 36 (Suppl 3):S13–9. [PubMed: 16188544]
2. Dwek JR. The periosteum: what is it, where is it, and what mimics it in its absence? Skeletal Radiol. 2010; 39(4):319–23. [PubMed: 20049593]
3. Ham AW. A histological study of the early phases of bone repair. J Bone Joint Surg. 1930; 12:827–44.
4. Hoffman MD, Benoit DS. Emerging ideas: Engineering the periosteum: revitalizing allografts by mimicking autograft healing. Clin Orthop Relat Res. 2013; 471(3):721–6. [PubMed: 23179118]

5. Hutmacher DW, Sittinger M. Periosteal cells in bone tissue engineering. Tissue Eng. 2003; 9 (Suppl 1):S45–64. [PubMed: 14511470]
6. Squier CA, Ghoneim S, Kremenak CR. Ultrastructure of the periosteum from membrane bone. J Anat. 1990; 171:233–9. [PubMed: 2081707]
7. Ellender G, Feik SA, Carach BJ. Periosteal structure and development in a rat caudal vertebra. J Anat. 1988; 158:173–87. [PubMed: 3225221]
8. Gnecchi M, Zhang Z, Ni A, Dzau VJ. Paracrine mechanisms in adult stem cell signaling and therapy. Circ Res. 2008; 103(11):1204–19. [PubMed: 19028920]
9. Chen L, Tredget EE, Wu PY, Wu Y. Paracrine factors of mesenchymal stem cells recruit macrophages and endothelial lineage cells and enhance wound healing. PLoS One. 2008; 3(4):e1886. [PubMed: 18382669]
10. Zhang X, Xie C, Lin AS, Ito H, Awad H, Lieberman JR, et al. Periosteal progenitor cell fate in segmental cortical bone graft transplantations: implications for functional tissue engineering. J Bone Miner Res. 2005; 20(12):2124–37. [PubMed: 16294266]
11. Xie C, Reynolds D, Awad H, Rubery PT, Pelled G, Gazit D, et al. Structural bone allograft combined with genetically engineered mesenchymal stem cells as a novel platform for bone tissue engineering. Tissue Eng. 2007; 13(3):435–45. [PubMed: 17518596]
12. Hoffman MD, Xie C, Zhang X, Benoit DS. The effect of mesenchymal stem cells delivered via hydrogel-based tissue engineered periosteum on bone allograft healing. Biomaterials. 2013; 34(35):8887–98. [PubMed: 23958029]
13. Devescovi V, Leonardi E, Ciapetti G, Cenni E. Growth factors in bone repair. Chir Organi Mov. 2008; 92(3):161–8. [PubMed: 19043663]
14. Burchardt H. The biology of bone graft repair. Clin Orthop Relat Res. 1983; (174):28–42. [PubMed: 6339139]
15. Burchardt H, Enneking WF. Transplantation of Bone. Surg Clin N Am. 1978; 58(2):403–27. [PubMed: 349741]
16. Burchardt H, Jones H, Glowczewskie F, Rudner C, Enneking WF. Freeze-dried allogeneic segmental cortical-bone grafts in dogs. J Bone Joint Surg Am. 1978; 60(8):1082–90. [PubMed: 363723]
17. Stevenson S, Shaffer JW, Goldberg VM. The humoral response to vascular and nonvascular allografts of bone. Clin Orthop Relat Res. 1996; (326):86–95. [PubMed: 8620663]
18. Stevenson S, Li XQ, Davy DT, Klein L, Goldberg VM. Critical biological determinants of incorporation of non-vascularized cortical bone grafts. Quantification of a complex process and structure. J Bone Joint Surg Am. 1997; 79(1):1–16. [PubMed: 9010181]
19. Mankin HJ, Gebhardt MC, Jennings LC, Springfield DS, Tomford WW. Long-term results of allograft replacement in the management of bone tumors. Clin Orthop Relat Res. 1996; (324):86–97. [PubMed: 8595781]
20. Granero-Molto F, Weis JA, Miga MI, Landis B, Myers TJ, O'Rear L, et al. Regenerative effects of transplanted mesenchymal stem cells in fracture healing. Stem Cells. 2009; 27(8):1887–98. [PubMed: 19544445]
21. Bielby R, Jones E, McGonagle D. The role of mesenchymal stem cells in maintenance and repair of bone. Injury. 2007; 38 (Suppl 1):S26–32. [PubMed: 17383482]
22. Chappuis V, Gamer L, Cox K, Lowery JW, Bosshardt DD, Rosen V. Periosteal BMP2 activity drives bone graft healing. Bone. 2012; 51(4):800–9. [PubMed: 22846673]
23. Derner R, Anderson AC. The bone morphogenic protein. Clin Podiatr Med Surg. 2005; 22(4):607–18. vii. [PubMed: 16213383]
24. Mattar T, Friedrich PF, Bishop AT. Effect of rhBMP-2 and VEGF in a vascularized bone allotransplant experimental model based on surgical neoangiogenesis. J Orthop Res. 2013; 31(4): 561–6. [PubMed: 23192572]
25. Deckers MM, van Bezooijen RL, van der Horst G, Hoogendam J, van Der Bent C, Papapoulos SE, et al. Bone morphogenetic proteins stimulate angiogenesis through osteoblast-derived vascular endothelial growth factor A. Endocrinology. 2002; 143(4):1545–53. [PubMed: 11897714]

26. Kempen DH, Creemers LB, Alblas J, Lu L, Verbout AJ, Yaszemski MJ, et al. Growth factor interactions in bone regeneration. Tissue Eng Part B Rev. 2010; 16(6):551–66. [PubMed: 21039299]
27. Bostrom MP, Lane JM, Berberian WS, Missri AA, Tomin E, Weiland A, et al. Immunolocalization and expression of bone morphogenetic proteins 2 and 4 in fracture healing. J Orthop Res. 1995; 13(3):357–67. [PubMed: 7602397]
28. Hanada K, Solchaga LA, Caplan AI, Hering TM, Goldberg VM, Yoo JU, et al. BMP-2 induction and TGF-beta 1 modulation of rat periosteal cell chondrogenesis. J Cell Biochem. 2001; 81(2): 284–94. [PubMed: 11241668]
29. Bouletreau PJ, Warren SM, Spector JA, Peled ZM, Gerrets RP, Greenwald JA, et al. Hypoxia and VEGF up-regulate BMP-2 mRNA and protein expression in microvascular endothelial cells: implications for fracture healing. Plast Reconstr Surg. 2002; 109(7):2384–97. [PubMed: 12045566]
30. Mayr-Wohlfart U, Waltenberger J, Hausser H, Kessler S, Gunther KP, Dehio C, et al. Vascular endothelial growth factor stimulates chemotactic migration of primary human osteoblasts. Bone. 2002; 30(3):472–7. [PubMed: 11882460]
31. Fiedler J, Leucht F, Waltenberger J, Dehio C, Brenner RE. VEGF-A and PlGF-1 stimulate chemotactic migration of human mesenchymal progenitor cells. Biochem Biophys Res Commun. 2005; 334(2):561–8. [PubMed: 16005848]
32. Ito H, Koefoed M, Tiyapatanaputi P, Gromov K, Goater JJ, Carmouche J, et al. Remodeling of cortical bone allografts mediated by adherent rAAV-RANKL and VEGF gene therapy. Nat Med. 2005; 11(3):291–7. [PubMed: 15711561]
33. Ma D, Yao H, Tian W, Chen F, Liu Y, Mao T, et al. Enhancing bone formation by transplantation of a scaffold-free tissue-engineered periosteum in a rabbit model. Clin Oral Implants Res. 2011; 22(10):1193–9. [PubMed: 21303418]
34. Schonmeyr B, Clavin N, Avraham T, Longo V, Mehrara BJ. Synthesis of a tissue-engineered periosteum with acellular dermal matrix and cultured mesenchymal stem cells. Tissue Eng Part A. 2009; 15(7):1833–41. [PubMed: 19125645]
35. Yu YY, Lieu S, Lu CY, Colnot C. Bone morphogenetic protein 2 stimulates endochondral ossification by regulating periosteal cell fate during bone repair. Bone. 2010; 47(1):65–73. [PubMed: 20348041]
36. Long T, Zhu Z, Awad HA, Schwarz EM, Hilton MJ, Dong Y. The effect of mesenchymal stem cell sheets on structural allograft healing of critical sized femoral defects in mice. Biomaterials. 2013; 35(9):2752–59. [PubMed: 24393269]
37. Huang C, Tang M, Yehling E, Zhang X. Overexpressing sonic hedgehog Peptide restores periosteal bone formation in a murine bone allograft transplantation model. Mol Ther. 2014; 22(2): 430–9. [PubMed: 24089140]
38. Huang YC, Kaigler D, Rice KG, Krebsbach PH, Mooney DJ. Combined angiogenic and osteogenic factor delivery enhances bone marrow stromal cell-driven bone regeneration. J Bone Miner Res. 2005; 20(5):848–57. [PubMed: 15824858]
39. Peng H, Wright V, Usas A, Gearhart B, Shen HC, Cummins J, et al. Synergistic enhancement of bone formation and healing by stem cell-expressed VEGF and bone morphogenetic protein-4. J Clin Invest. 2002; 110(6):751–9. [PubMed: 12235106]
40. Samee M, Kasugai S, Kondo H, Ohya K, Shimokawa H, Kuroda S. Bone morphogenetic protein-2 (BMP-2) and vascular endothelial growth factor (VEGF) transfection to human periosteal cells enhances osteoblast differentiation and bone formation. J Pharmacol Sci. 2008; 108(1):18–31. [PubMed: 18776714]
41. Awad HA, Zhang X, Reynolds DG, Guldberg RE, O'Keefe RJ, Schwarz EM. Recent advances in gene delivery for structural bone allografts. Tissue Eng. 2007; 13(8):1973–85. [PubMed: 17518728]
42. Takahata M, Awad HA, O'Keefe RJ, Bukata SV, Schwarz EM. Endogenous tissue engineering: PTH therapy for skeletal repair. Cell Tissue Res. 2012; 347(3):545–52. [PubMed: 21626290]

43. Cao L, Liu X, Liu S, Jiang Y, Zhang X, Zhang C, et al. Experimental repair of segmental bone defects in rabbits by angiopoietin-1 gene transfected MSCs seeded on porous beta-TCP scaffolds. J Biomed Mater Res B Appl Biomater. 2012; 100(5):1229–36. [PubMed: 22576851]
44. Han SK, Yoon TH, Lee DG, Lee MA, Kim WK. Potential of human bone marrow stromal cells to accelerate wound healing in vitro. Ann Plast Surg. 2005; 55(4):414–9. [PubMed: 16186710]
45. Allen MR, Hock JM, Burr DB. Periosteum: biology, regulation, and response to osteoporosis therapies. Bone. 2004; 35(5):1003–12. [PubMed: 15542024]
46. Hsiao ST, Asgari A, Lokmic Z, Sinclair R, Dusting GJ, Lim SY, et al. Comparative analysis of paracrine factor expression in human adult mesenchymal stem cells derived from bone marrow, adipose, and dermal tissue. Stem Cells Dev. 2012; 21(12):2189–203. [PubMed: 22188562]
47. Brudno Y, Ennett-Shepard AB, Chen RR, Aizenberg M, Mooney DJ. Enhancing microvascular formation and vessel maturation through temporal control over multiple pro-angiogenic and pro-maturation factors. Biomaterials. 2013; 34(36):9201–9. [PubMed: 23972477]
48. Hou H, Zhang X, Tang T, Dai K, Ge R. Enhancement of bone formation by genetically-engineered bone marrow stromal cells expressing BMP-2, VEGF and angiopoietin-1. Biotechnol Lett. 2009; 31(8):1183–9. [PubMed: 19390786]
49. Xiao Y, Haase H, Young WG, Bartold PM. Development and transplantation of a mineralized matrix formed by osteoblasts in vitro for bone regeneration. Cell Transplant. 2004; 13(1):15–25. [PubMed: 15040601]
50. Sawhney AS, Pathak CP, Hubbell JA. Bioerodible hydrogels based on photopolymerized poly(ethylene glycol)-co-poly(alpha-hydroxy acid) diacrylate macromers. Macromolecules. 1993; 26(4):581–7.
51. Hoffman MD, Benoit DS. Agonism of Wnt-beta-catenin signalling promotes mesenchymal stem cell (MSC) expansion. J Tissue Eng Regen Med. In Press.
52. Lin-Gibson S, Bencherif S, Cooper JA, Wetzel SJ, Antonucci JM, Vogel BM, et al. Synthesis and characterization of PEG dimethacrylates and their hydrogels. Biomacromolecules. 2004; 5(4): 1280–7. [PubMed: 15244441]
53. Van Hove AH, Wilson BD, Benoit DSW. Microwave-assisted Functionalization of Poly(ethylene glycol) and On-resin Peptides for Use in Chain Polymerizations and Hydrogel Formation. JOVE. 2013; 80(e50890):1–16.
54. Benoit DS, Boutin ME. Controlling mesenchymal stem cell gene expression using polymer-mediated delivery of siRNA. Biomacromolecules. 2012; 13(11):3841–9. [PubMed: 23020123]
55. Jaiswal N, Haynesworth SE, Caplan AI, Bruder SP. Osteogenic differentiation of purified, culture-expanded human mesenchymal stem cells in vitro. J Cell Biochem. 1997; 64(2):295–312. [PubMed: 9027589]
56. Tiyapatanaputi P, Rubery PT, Carmouche J, Schwarz EM, O'Keefe RJ, Zhang X. A novel murine segmental femoral graft model. J Orthop Res. 2004; 22(6):1254–60. [PubMed: 15475206]
57. Benoit DS, Tripodi MC, Blanchette JO, Langer SJ, Leinwand LA, Anseth KS. Integrin-linked kinase production prevents anoikis in human mesenchymal stem cells. J Biomed Mater Res A. 2007; 81(2):259–68. [PubMed: 17335036]
58. Benoit DSW, Collins SD, Anseth KS. Multifunctional hydrogels that promote osteogenic human mesenchymal stem cell differentiation through stimulation and sequestering of bone morphogenic protein 2. Adv Funct Mater. 2007; 17(13):2085–93. [PubMed: 18688288]
59. Benoit DSW, Schwartz MP, Durney AR, Anseth KS. Small functional groups for controlled differentiation of hydrogel-encapsulated human mesenchymal stem cells. Nat Mater. 2008; 7(10): 816–23. [PubMed: 18724374]
60. Fairbanks BD, Schwartz MP, Bowman CN, Anseth KS. Photoinitiated polymerization of PEG-diacrylate with lithium phenyl-2,4,6-trimethylbenzoylphosphinate: polymerization rate and cytocompatibility. Biomaterials. 2009; 30(35):6702–7. [PubMed: 19783300]
61. Nuttelman CR, Tripodi MC, Anseth KS. Synthetic hydrogel niches that promote hMSC viability. Matrix Biol. 2005; 24(3):208–18. [PubMed: 15896949]
62. Duvall CL, Taylor WR, Weiss D, Guldberg RE. Quantitative microcomputed tomography analysis of collateral vessel development after ischemic injury. Am J Physiol Heart Circ Physiol. 2004; 287(1):H302–10. [PubMed: 15016633]

63. Jiang X, Kalajzic Z, Maye P, Braut A, Bellizzi J, Mina M, et al. Histological analysis of GFP expression in murine bone. J Histochem Cytochem. 2005; 53(5):593–602. [PubMed: 15872052]
64. Hassan MQ, Tare RS, Lee SH, Mandeville M, Morasso MI, Javed A, et al. BMP2 commitment to the osteogenic lineage involves activation of Runx2 by DLX3 and a homeodomain transcriptional network. J Biol Chem. 2006; 281(52):40515–26. [PubMed: 17060321]
65. Hattori T, Muller C, Gebhard S, Bauer E, Pausch F, Schlund B, et al. SOX9 is a major negative regulator of cartilage vascularization, bone marrow formation and endochondral ossification. Development. 2010; 137(6):901–11. [PubMed: 20179096]
66. Kenyon NJ, Ward RW, McGrew G, Last JA. TGF-beta1 causes airway fibrosis and increased collagen I and III mRNA in mice. Thorax. 2003; 58(9):772–7. [PubMed: 12947136]
67. Park GT, Morasso MI. Bone morphogenetic protein-2 (BMP-2) transactivates Dlx3 through Smad1 and Smad4: alternative mode for Dlx3 induction in mouse keratinocytes. Nucleic Acids Res. 2002; 30(2):515–22. [PubMed: 11788714]
68. Pfaffl MW. A new mathematical model for relative quantification in real-time RT-PCR. Nucleic Acids Res. 2001; 29(9):e45. [PubMed: 11328886]
69. Reynolds DG, Hock C, Shaikh S, Jacobson J, Zhang X, Rubery PT, et al. Micro-computed tomography prediction of biomechanical strength in murine structural bone grafts. J Biomech. 2007; 40(14):3178–86. [PubMed: 17524409]
70. Brodt MD, Ellis CB, Silva MJ. Growing C57Bl/6 mice increase whole bone mechanical properties by increasing geometric and material properties. J Bone Miner Res. 1999; 14(12):2159–66. [PubMed: 10620076]
71. Reynolds DG, Shaikh S, Papuga MO, Lerner AL, O'Keefe RJ, Schwarz EM, et al. muCT-based measurement of cortical bone graft-to-host union. J Bone Miner Res. 2009; 24(5):899–907. [PubMed: 19063685]
72. Colnot C. Skeletal Cell Fate Decisions Within Periosteum and Bone Marrow During Bone Regeneration (vol 24, pg 274, 2009). Journal of Bone and Mineral Research. 2009; 24(4):758.
73. Nie H, Ho ML, Wang CK, Wang CH, Fu YC. BMP-2 plasmid loaded PLGA/HAp composite scaffolds for treatment of bone defects in nude mice. Biomaterials. 2009; 30(5):892–901. [PubMed: 19010530]
74. Henriksen K, Karsdal M, Delaisse JM, Engsig MT. RANKL and vascular endothelial growth factor (VEGF) induce osteoclast chemotaxis through an ERK1/2-dependent mechanism. J Biol Chem. 2003; 278(49):48745–53. [PubMed: 14506249]
75. Dhillon RS, Xie C, Tyler W, Calvi LM, Awad HA, Zuscik MJ, et al. PTH-enhanced structural allograft healing is associated with decreased angiopoietin-2-mediated arteriogenesis, mast cell accumulation, and fibrosis. J Bone Miner Res. 2013; 28(3):586–97. [PubMed: 22991274]
76. Udani V, Santarelli J, Yung Y, Cheshier S, Andrews A, Kasad Z, et al. Differential expression of angiopoietin-1 and angiopoietin-2 may enhance recruitment of bone-marrow-derived endothelial precursor cells into brain tumors. Neurol Res. 2005; 27(8):801–6. [PubMed: 16354539]
77. Lienau J, Schmidt-Bleek K, Peters A, Haschke F, Duda GN, Perka C, et al. Differential regulation of blood vessel formation between standard and delayed bone healing. J Orthop Res. 2009; 27(9): 1133–40. [PubMed: 19274756]
78. Patel ZS, Young S, Tabata Y, Jansen JA, Wong ME, Mikos AG. Dual delivery of an angiogenic and an osteogenic growth factor for bone regeneration in a critical size defect model. Bone. 2008; 43(5):931–40. [PubMed: 18675385]
79. Peng H, Usas A, Olshanski A, Ho AM, Gearhart B, Cooper GM, et al. VEGF improves, whereas sFlt1 inhibits, BMP2-induced bone formation and bone healing through modulation of angiogenesis. J Bone Miner Res. 2005; 20(11):2017–27. [PubMed: 16234975]
80. Zhang WJ, Wang XL, Wang SY, Zhao J, Xu LY, Zhu C, et al. The use of injectable sonication-induced silk hydrogel for VEGF(165) and BMP-2 delivery for elevation of the maxillary sinus floor. Biomaterials. 2011; 32(35):9415–24. [PubMed: 21889205]
81. Taguchi K, Ogawa R, Migita M, Hanawa H, Ito H, Orimo H. The role of bone marrow-derived cells in bone fracture repair in a green fluorescent protein chimeric mouse model. Biochem Biophys Res Commun. 2005; 331(1):31–6. [PubMed: 15845353]

82. Tsuji K, Bandyopadhyay A, Harfe BD, Cox K, Kakar S, Gerstenfeld L, et al. BMP2 activity, although dispensable for bone formation, is required for the initiation of fracture healing. Nat Genet. 2006; 38(12):1424–9. [PubMed: 17099713]

83. Yazici C, Takahata M, Reynolds DG, Xie C, Samulski RJ, Samulski J, et al. Self-complementary AAV2.5-BMP2-coated femoral allografts mediated superior bone healing versus live autografts in mice with equivalent biomechanics to unfractured femur. Mol Ther. 2011; 19(8):1416–25. [PubMed: 21206485]

84. Mountziaris PM, Mikos AG. Modulation of the inflammatory response for enhanced bone tissue regeneration. Tissue Eng Part B Rev. 2008; 14(2):179–86. [PubMed: 18544015]

85. Suzuki T, Miyamoto T, Fujita N, Ninomiya K, Iwasaki R, Toyama Y, et al. Osteoblast-specific Angiopoietin 1 overexpression increases bone mass. Biochem Biophys Res Commun. 2007; 362(4):1019–25. [PubMed: 17825261]

86. Van Hove AH, Beltejar MJG, Benoit DSW. Development and in vitro assessment of enzymatically-responsive poly(ethylene glycol) hydrogels for the delivery of therapeutic peptides. Biomaterials. 2014; 35(36):9719–30. [PubMed: 25178558]

87. Benoit DSW, Anseth KS. Heparin functionalized PEG gels that modulate protein adsorption for hMSC adhesion and differentiation. Acta Biomater. 2005; 1(4):461–70. [PubMed: 16701827]

88. Benoit DSW, Durney AR, Anseth KS. The effect of heparin-functionalized PEG hydrogels on three-dimensional human mesenchymal stem cell osteogenic differentiation. Biomaterials. 2007; 28(1):66–77. [PubMed: 16963119]

89. Benoit DSW, Nuttelman CR, Collins SD, Anseth KS. Synthesis and characterization of a fluvastatin-releasing hydrogel delivery system to modulate hMSC differentiation and function for bone regeneration. Biomaterials. 2006; 27(36):6102–10. [PubMed: 16860387]

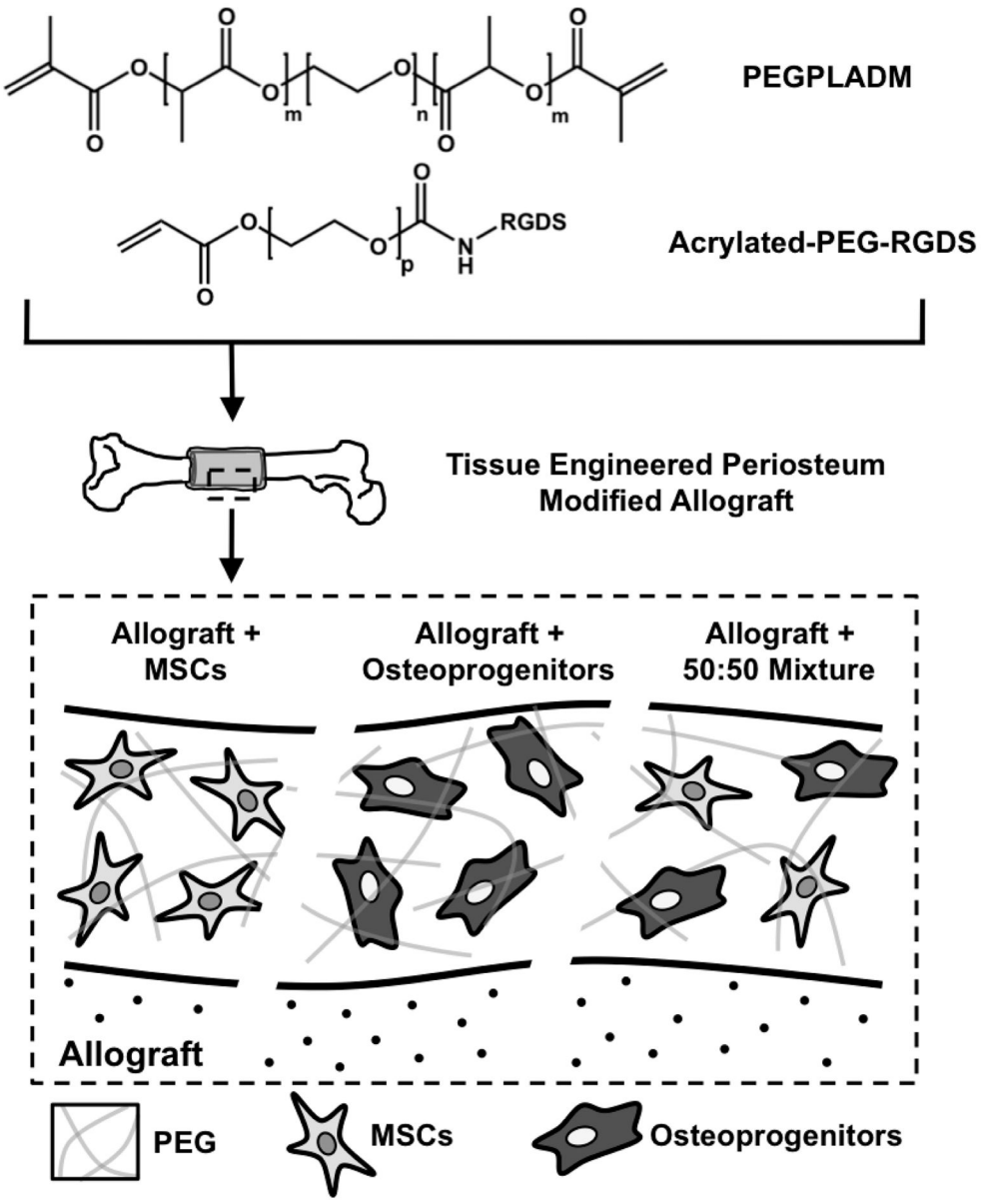

Figure 1.

Schematic representation of the poly(ethylene glycol) (PEG) based tissue engineered periosteum. Hydrolytically degradable PEG macromers (n=227, m=3, p=79) were utilized to photopolymerize MSCs, osteoprogenitors, or a 50:50 mixed combination thereof around decellularized allografts using custom molds to fabricate tissue engineered periosteum modified allografts.

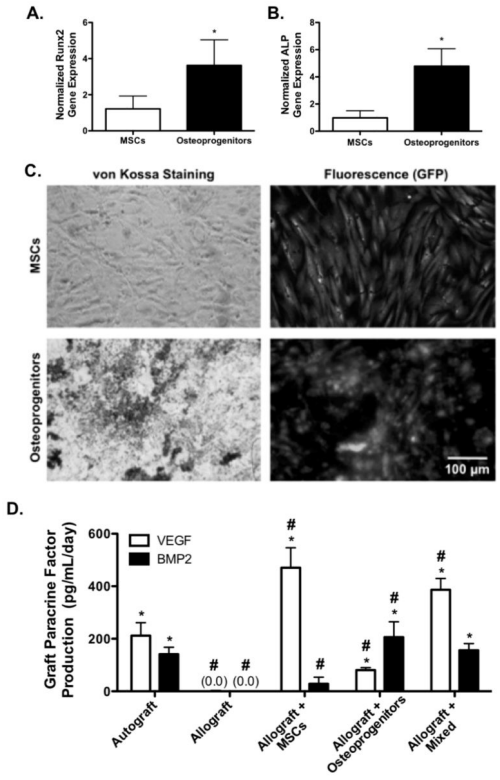

Figure 2.

Gene analysis for markers of osteogenesis (Cbfa1; A, ALP; B) and histological assessment of mineralization (von Kossa, hydroxyapatite; C) of GFP^+ MSCs following 10 days of osteogenic differentiation (n=6; error bars represent standard deviation; *p*-value of <0.05 indicates significance compared to controls (*)). Quantification of graft vascular endothelial growth factor (VEGF) and bone morphogenetic protein-2 (BMP2) paracrine factor production showed that tissue engineered periosteum modified allografts transplanting a mixed population of MSCs and osteoprogenitors best matched paracrine release profiles of autograft controls (D) (n=5–7; error bars represent standard deviation; *p*-value of <0.05 indicates significance compared to allograft (*) or autograft (#)).

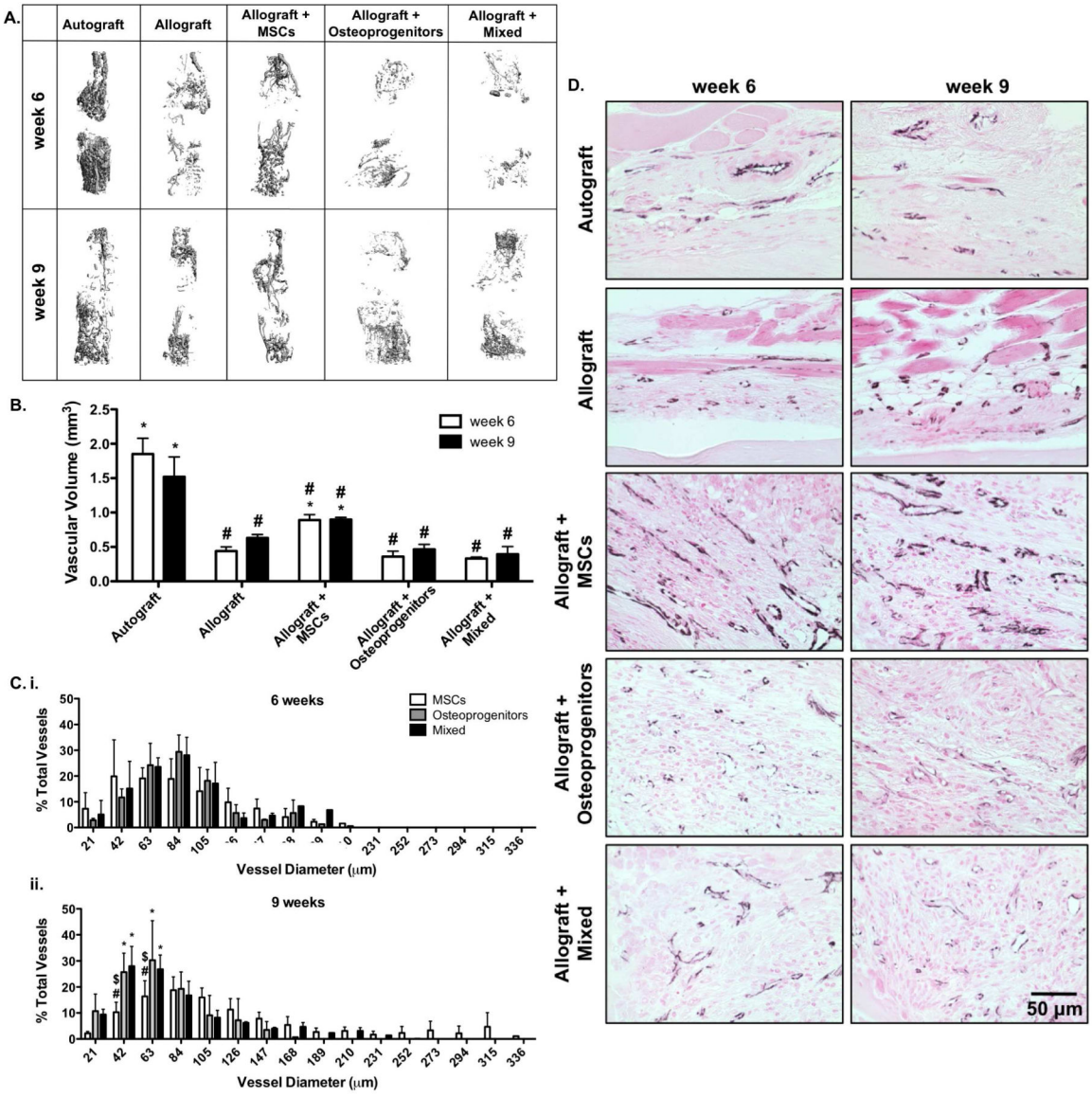

Figure 3.

Micro-computed tomography (μCT) scans taken 6 and 9 weeks post-implantation were reconstructed to assess *in vivo* host-mediated graft vascular infiltration (A). Subsequent quantification revealed that tissue engineered periosteum modified allografts transplanting a combination of MSCs and osteoprogenitors, or osteoprogenitors alone exhibited reduced vascular volume as compared to transplantation of MSCs alone (B) (n=6; error bars represent standard error of the mean; *p*-value of <0.05 indicates significance compared to allograft (*) or autograft (#)). This reduction in total vascular volume was shown to be due to decreased arteriogenesis and increased small vessel formation; as verified by micro-computed tomography thresholding (C) (n=6; error bars represent standard deviation; *p*-value of <0.05 indicates significance compared to MSCs (*), mixed (#), or osteoprogenitors ($)), and immunohistological staining for CD31 (D) (black; CD31, and pink; nuclear fast red counter stain and muscle).

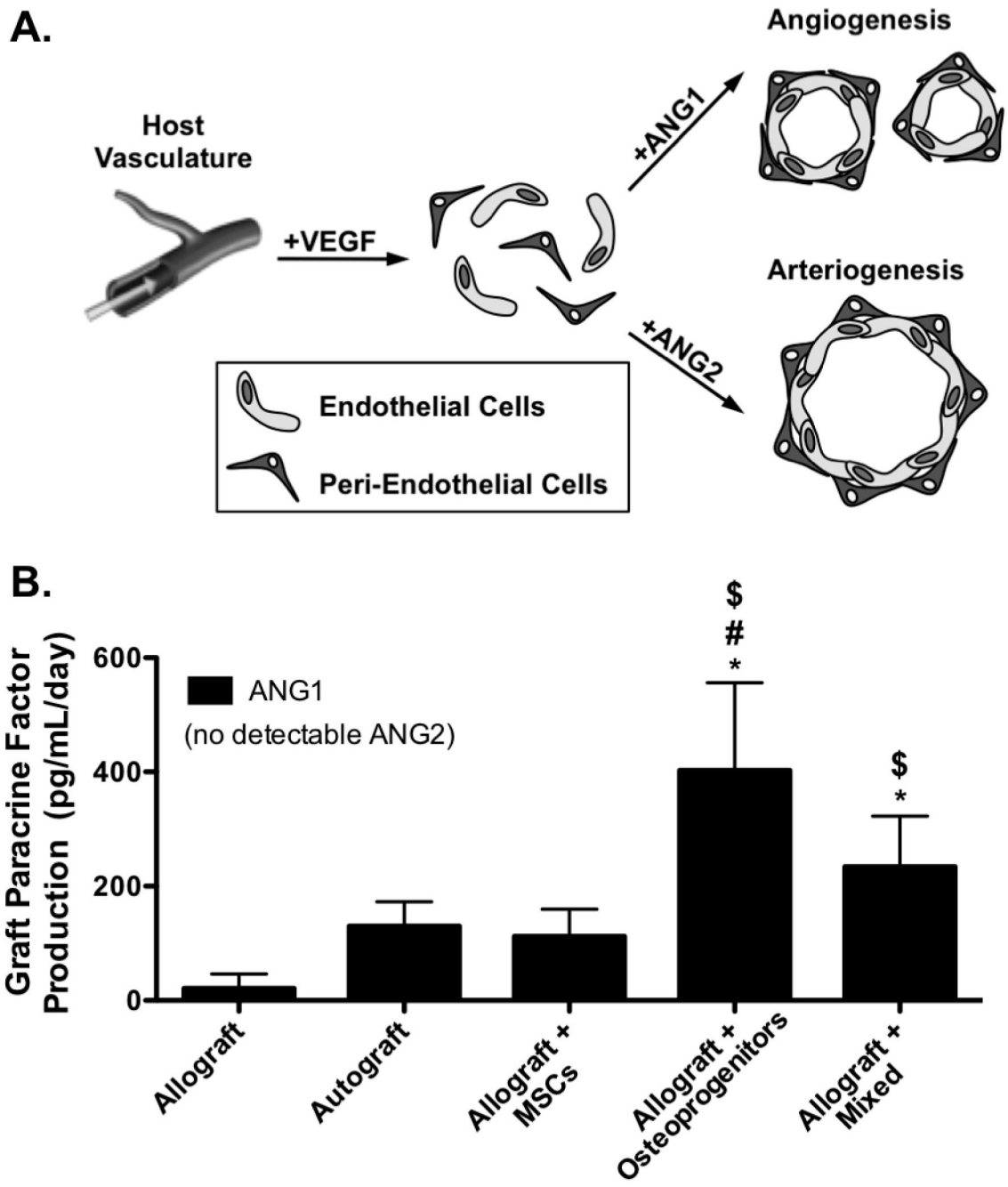

Figure 4.

Schematic representation of paracrine mediated vascular infiltration in which angiopoietin 1 (ANG1) drives small vessel angiogenesis while angiopoietin 2 (ANG2) drives vascular remodeling and promotes large vessel arteriogenesis (A). Quantification revealed that tissue engineered periosteum modified allografts transplanting a mixed cell population, or osteoprogenitors alone resulted in a significant increase in ANG1 production, as compared to transplantation of MSCs alone (B) (n=5–7; error bars represent standard deviation; *p*-

value of <0.05 indicates significance compared to allograft (*), autograft (#), or allograft + MSCs ($)).

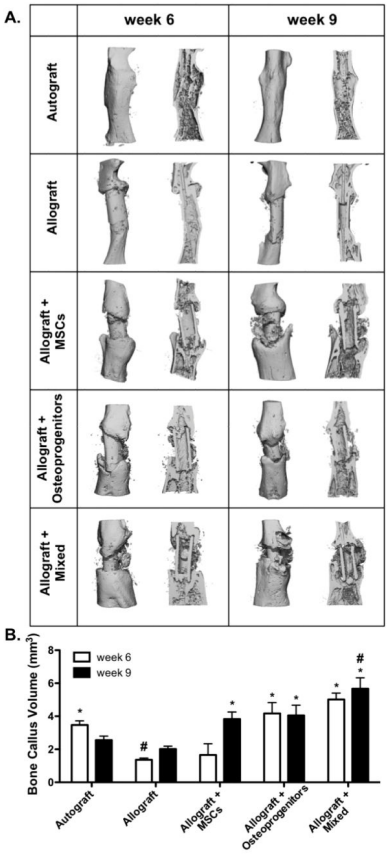

Figure 5.

Micro-computed tomography (μCT) scans taken 6 and 9 weeks post-implantation were reconstructed to assess *in vivo* bone callus formation (A; intact and sagital cut views). Subsequent quantification revealed that tissue engineered periosteum modified allografts transplanting a mixed cell population significantly increased bone callus volume as compared to transplantation of either MSCs or osteoprogenitors alone, as well as allograft only controls (B) (n=5–6; error bars represent standard error of the mean; *p*-value of <0.05 indicates significance compared to allograft (*) or autograft (#)).

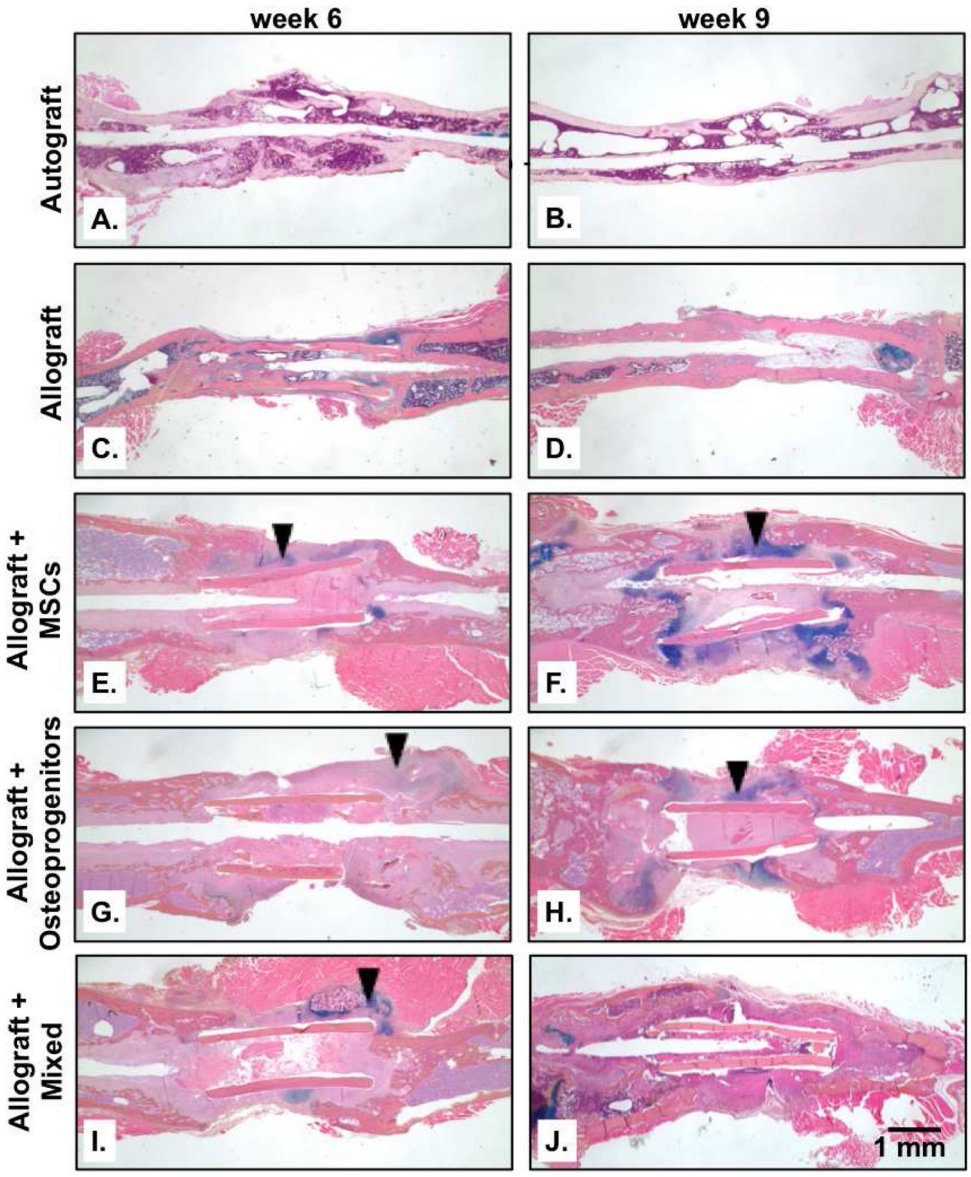

Figure 6.

Histological analysis of graft sections was performed using alcian blue (blue; glycosaminoglycans and proteoglycans) and orange G staining (pink; bone and surrounding soft tissue) (A–J). T.E. periosteum modified allografts transplanting a mixed cell population were shown to have significantly reduced bridging cartilaginous matrix staining (black arrows) as compared to T.E. periosteum modified allografts transplanting only MSCs or osteoprogenitors.

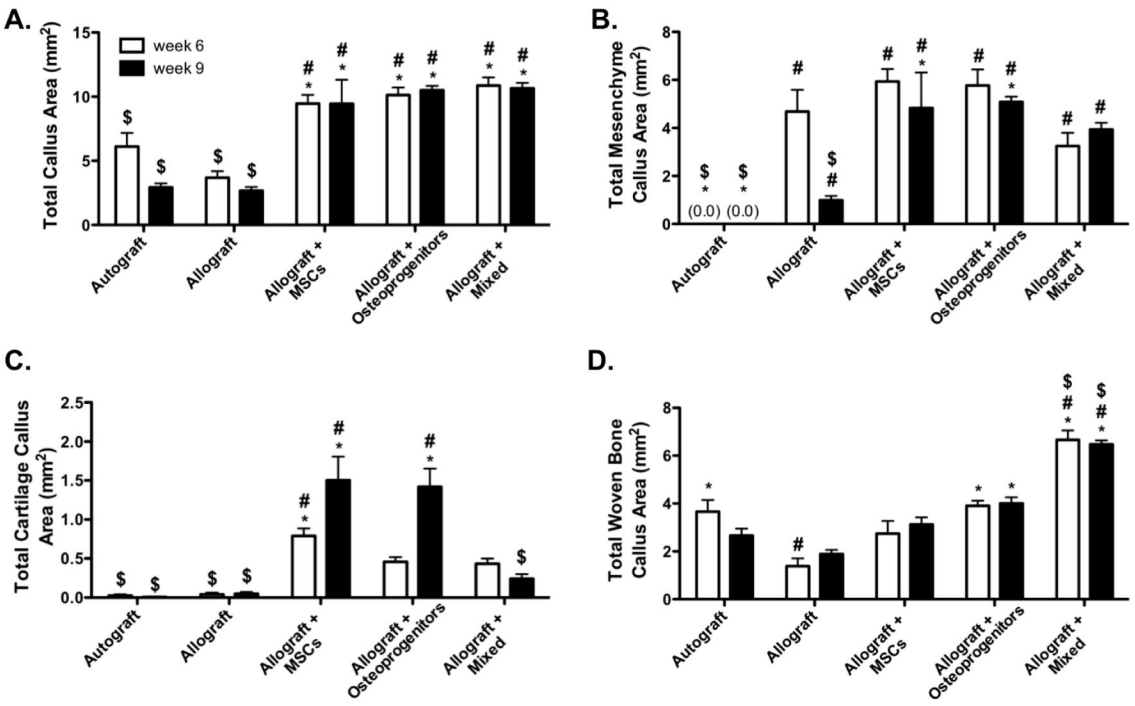

Figure 7.

Histomorphometric analysis of stained graft sections (Fig. 5) revealed a comparable total callus area (A), but a decrease in total mesenchyme callus (B) and total cartilage callus (C) area, and an increase in total woven bone callus (D) area in tissue engineered periosteum modified allografts transplanting a mixed cell population as compared to transplantation of either MSCs or osteoprogenitors (n=10; error bars represent standard error of the mean; *p*-value of <0.05 indicates significance compared to allograft (*), autograft (#), or allograft + MSCs ($)).

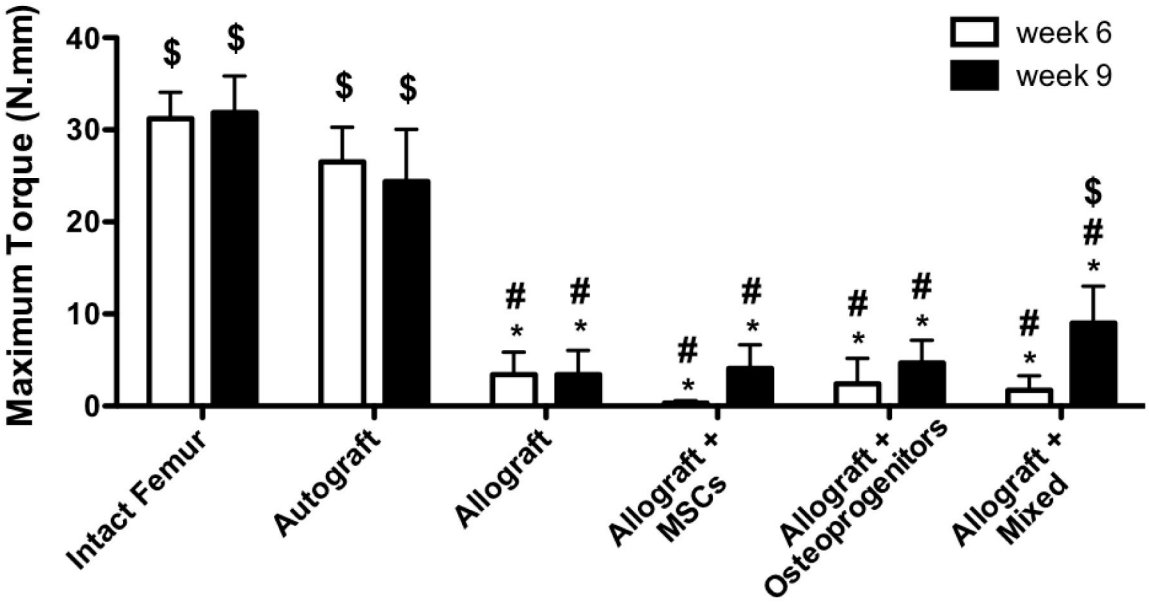

Figure 8.

Maximal torsion strength of tissue engineered periosteum modified allografts transplanting a mixed cell population was significantly increased over unmodified allograft controls, and tissue engineered periosteum modified allografts transplanting either MSCs or osteoprogenitors 9 weeks post-implantation (n=8–10; error bars represent standard error of the mean; *p*-value of <0.05 indicates significance compared to intact femur (*), autograft (#), or allograft ($)).

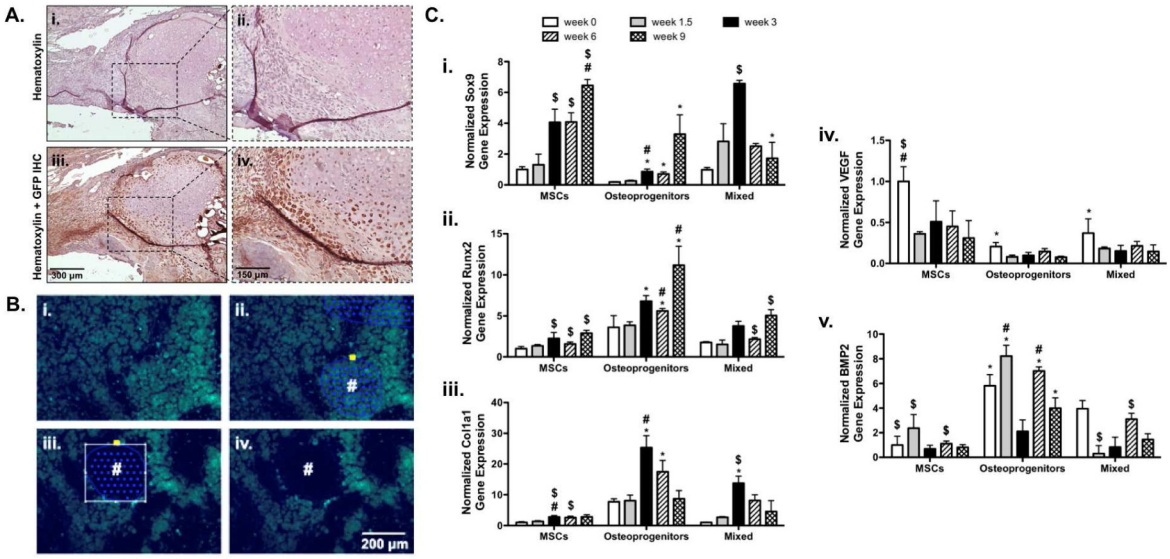

Figure 9.

Representative immunohistological staining for green fluorescent protein (GFP) showed limited incorporation of mixed (GFP^+ mMSCs and osteoprogenitors) into the newly formed bone callus 9 weeks post-implantation (A). Despite this finding, fluorescence microscopy was used to locate transplanted mixed GFP^+ mMSCs and osteoprogenitors within prepared histological sections (B) and laser capture microdissection (LCM) was performed to remove selected cells (#; Ci–Civ). Subsequent RNA isolation and gene expression analysis revealed that cells transplanted in a 50:50 ratio of MSCs to osteoprogenitors exhibited trends towards expedited endochondral ossification as determined by Sox9 (Ci.), Runx2 (Cii.), Col1a1 (Ciii.), VEGF (Civ), and BMP2 (Cv) gene expression (n=5–6; error bars represent standard error of the mean; *p*-value of <0.05 indicates significance compared to MSCs (*), 50:50 MSCs (#), or osteogenic MSCs ($)).

Table 1

Quantification of micro-computed tomography callus bone volume (Fig. 5) revealed trends towards increased percent graft-host connectivity (union ratio) 9 weeks post-implantation for tissue engineered periosteum modified allografts transplanting a mixed cell population, following the same trend as observed in total woven callus bone area (Fig. 6D) and torsional biomechanics (Fig. 7) (n=5–7; error bars represent standard error of the mean; *p*-value of <0.05 indicates significance compared to allograft (*) or autograft (#)).

	Autograft	Allograft	Allograft + MSCs	Allograft + Osteoprogenitors	Allograft + Mixed
week 6	20.7 ± 2.9%	12.3 ± 1.7%	11.2 ± 1.6%[#]	10.9 ± 1.9%[#]	13.9 ± 1.6%
week 9	16.0 ± 0.7%	13.9 ± 2.2%	15.9 ± 2.9%	15.4 ± 1.1 %	19.3 ± 0.8%